Korean J. Chem. Eng., 39(1), 109-115 (2022)
DOI: 10.1007/s11814-021-0988-9

pISSN: 0256-1115
eISSN: 1975-7220

Coupling of nitrobenzene hydrogenation and 1, 4-butanediol dehydrogenation for the simultaneous synthesis of aniline and γ-butyrolactone over copper-based catalysts

Veeralakshmi Vaddeboina*, Hari Prasad Reddy Kannapu,†, Jong-Ki Jeon***, Young-Kwon Park**,†, and Kuthati Bhaskar*,†**

*Department of Chemistry, Osmania University, Hyderabad-500007, India
**School of Environmental Engineering, University of Seoul, Seoul 02504, Korea
***Department of Chemical Engineering, Kongju National University, Cheonan 31081, Korea
(*Received 23 June 2021 • Revised 22 September 2021 • Accepted 18 October 2021*)

Abstract−This study examined the role of the support material on the coupling of 1,4-butanediol (BDO) dehydrogenation and nitrobenzene (NB) hydrogenation over copper-based catalysts. The catalysts, 10Cu/MgO (10CM), 10Cu/Al_2O_3 (10CA), 10Cu/MgO-Al_2O_3 (10CMA), and 10Cu/SiO_2 (10CS), were prepared using the impregnation method. The coupling reaction results conducted at 250 °C were compared with those of the individual reactions. The individual BDO dehydrogenation to γ-butyrolactone (GBL) conversion (99%) and hydrogenation of NB to aniline (AN) conversion (85 %) were high over 10CS. In contrast, 10CA produced tetrahydrofuran (THF) as a major product from BDO. Interestingly, the coupling process over the 10CM catalyst produced the best performance in converting NB (65%) to AN (99%) and BDO (85%) to GBL (99%). The superior performance of Cu/MgO in coupling process catalyst is mainly due to the high hydrogen adsorption ability compared to the other catalysts under limited hydrogen environments, which helps retain the active hydrogen on the catalyst surface for a longer time. The characterization of the catalysts showed that a high basic nature and the optimal amount of active copper sites (Cu^0/Cu^{1+}) are responsible for the best performance of 10CM, followed by 10CS and 10CMA.

Keywords: Hydrogenation, Dehydrogenation, Aniline, γ-Butyrolactone, Cu, Support

INTRODUCTION

Simultaneous dehydrogenation and hydrogenation reactions are of great importance because of hydrogen atom efficiency. This technology has recently attracted considerable attention because of its enormous advantages in energy saving, catalyst development, and time saving [1]. Aniline (AN) is one of the most versatile chemicals for synthesizing plastics and agricultural products. It is produced mainly from the hydrogenation of nitrobenzene (NB) under noble metal catalysts with high-pressure hydrogen and high temperatures [2,3]. However, the entire process is expensive and not economically feasible. Therefore, non-noble metals, such as Ni, Co, and Cu, deposited on both acidic and basic supports, have shown superior performance [4-6]. Acid and base support materials play major roles in the catalytic hydrogenation of NB to AN via either the homolytic or heterolytic dissociation of hydrogen or both on an active metal and support [7].

The cyclic dehydrogenation of 1,4-butanediol (BDO) to γ-butyrolactone (GBL) only releases hydrogen. GBL has many industrial applications, including as a green solvent and additives for rubber synthesis [8]. Moreover, the hydrogen formed from alcohols can be used directly for various routes, such as green fuels and hydrogenating agents [7,9]. Despite the enormous advantages of this reaction, GBL is generally synthesized from the hydrogenation of succinic acid and maleic anhydride [10,11] over ruthenium and mixed oxide catalysts or a combination of noble and non-noble metals (Pd-Mo-Ni/SiO_2 and Ru-Ni/SiO_2) in a batch-type reactor system by inserting an external hydrogen source, which is undesirable.

The coupling of BDO dehydrogenation and NB hydrogenation reactions would be an alternative method to produce AN and GBL without an external hydrogen source. The selection of a suitable support is a crucial step for developing highly active and stable catalysts. Dezhi et al. examined maleic anhydride hydrogenation with 2-butanol dehydrogenation over various supported copper catalysts, such as Cu/ZrO_2, Cu-ZnO, and Cu-Al_2O_3 [12,13]. On the other hand, the copper sites in Cu/Al_2O_3 favor the dehydrogenation of ethanol to acetaldehyde, whereas the acid sites of alumina favor ethyl acetate (condensation), which is undesirable. Moreover, the behavior of Cu-Al_2O_3 for alcohols varies according to the type of alcohol. For example, tetrahydrofurfuryl alcohol is converted to dihydropyran via rearrangement followed by dehydration [14]. In the case of the coupling of NB hydrogenation to AN using 2-butanol over Cu/SiO_2, 100% yields of the desired products were obtained [15] because the side reactions of 2-butanol were controlled by the less acidic nature of SiO_2. A previous study on the use of mixed oxide catalyst, MgO-Al_2O_3 supported Ag, for the coupling of ethanol to n-butanol delineated the role of the acid and base sites in the catalyst [16]. The final product formation took place mainly in two steps: (i) dehydrogenation of ethanol to acetaldehyde, and

†To whom correspondence should be addressed.
E-mail: kannapu83@uos.ac.kr, catalica@uos.ac.kr, kuthati18@osmania.ac.in

(ii) aldehyde reaction with alcohols to convert n-propanol. These results showed that a combination of both basic and acidic supports provided new active sites to produce the desired product by suppressing unwanted side reactions. Similarly, the MgO support is a strong base with dehydrogenation capability without an active metal [17]. Hence, the dehydrogenation of alcohols plays a promising role in coupling reactions when they do not involve side reactions, such as condensation and dehydration. Based on the above reactions, the acid/base supports effectively altered the directions of the reaction pathway depending on the type of reactions.

In our previous studies, the simultaneous production of AN and GBL from NB hydrogenation and BDO dehydrogenation, respectively, revealed the role of copper and MgO [6]. Very recently, the effect of promoters on Cu-MgO was examined for long-term stability in which the promoter enhanced the copper dispersion, metal-support interactions and surface area of catalysts [9]. Moreover, copper (Cu^0/Cu^{+1}) sites played a major role in both dehydrogenation and hydrogenation reactions. However, the cause of deactivation in long-term study is oxidation of copper sites (Cu^+/Cu^0) to CuO with water molecules from the reaction and decrease of surface area by agglomeration of metal and support particles with continuing exposure at high temperature [18]. Therefore, to stabilize the copper particles and provide the high surface in the catalytic systems, we employed different supports which are active for hydrogenation of NB to AN under external hydrogen and dehydrogenation of BDO to GBL individually. Therefore, Al_2O_3 and SiO_2 and MgO-Al_2O_3 along with MgO support were selected. MgO is an interesting metal oxide that can make hydrogen adsorb in the form of proton (H^+) and hydride (H^-). This was confirmed by Coluccia et al. using infrared study of hydrogen adsorption over MgO, SrO and CaO [19]. Further, Wu et al. explained detailed hydrogen adsorption and dissociation over MgO surface using the density functional theory studies [20]. In this study, H_2 molecule was interacted with MgO (001) surface via four different methods: (i) directly on-top of a magnesium atom (on-top(Mg) site); (ii) directly on-top of an oxygen atom (on-top(O) site); (iii) at the middle of two nearest neighbor magnesium and oxygen atoms (bridge site); and (iv) at the center of the smallest unit structures of the surfaces (center site). In a recent study, Kim et al. developed MgO supported Ru catalysts for low temperature hydrogen storage in poly aromatics via hydrogenation [7]. This study also proved the hydrogen homolytic and heterolytic adsorption on Ru/MgO rather Ru/Al_2O_3 [7]. The reason to select different support is that Al_2O_3 acts as an amphoteric, SiO_2 acts as a slightly acidic, and MgO-Al_2O_3 acts as basic support. Moreover, SiO_2 exhibits hydrophobic nature which minimizes the oxidation of copper [21] and MgO-Al_2O_3 mixed oxide turn to be hydrotalcite in the presence of water, which is called memory effect [22]. To the best of our knowledge, the role of supports has not been studied for simultaneous hydrogenation and dehydrogenation of the present reaction.

The present study reports the effects of the supports on the coupling of NB hydrogenation and BDO dehydrogenation over Cu/MgO, Cu/Al_2O_3, Cu/MgO-Al_2O_3, and Cu/SiO_2 catalysts produced using the impregnation method. Individual hydrogenation and dehydrogenation reactions were carried out along with the coupling reaction to compare the final results. All catalysts were characterized using various analytical techniques, such Brunauer-Emmett-Teller (BET) surface area, X-ray fluorescence (XRF) spectroscopy, X-ray diffraction (XRD), N_2O pulse chemisorption, temperature-programmed desorption (TPD) of NH_3 and X-ray photoelectron spectroscopy (XPS), to examine the reaction sites for the above coupling processes.

EXPERIMENTAL

1. Preparation of Catalysts

Initially, the supports employed in the present study, such as MgO, and γ-Al_2O_3, were prepared using the precipitation method and Mg-Al was prepared by co-precipitation, but fumed silica was purchased from Sigma Chemicals (M/s Sigma-Aldrich). For the synthesis of MgO, an aqueous Mg $(NO_3)_2 \cdot 6H_2O$ solution was precipitated using a 10 wt% Na_2CO_3 solution as a precipitating agent by dropwise addition until pH 10. Subsequently, the white gel was filtered and washed with distilled water until pH 7. The sample was then dried and calcined at 450 °C for 5 h in the open air. Similarly, γ-Al_2O_3 was prepared using Al $(NO_3)_3 \cdot 9H_2O$ as an alumina precursor. For MgO-Al_2O_3 (2 : 1), the following procedure was applied. Briefly, the following solutions were prepared separately: solution A containing a mixture of 256 g of Mg $(NO_3)_2 \cdot 6H_2O$ and 185.7 g of Al $(NO_3)_3 \cdot 9H_2O$ in distilled water, and solution B containing 280 g of 50% NaOH (140 g in 140 cm^3 distilled water) and 100 g of Na_2CO_3 in 1,000 cm^3 distilled water. Subsequently, solution A was added dropwise to solution B over 3 h with constant stirring while maintaining the pH between 11 and 13. The final sample was transferred to an autoclave and allowed to crystallize at 60 °C for 18 h. The sample was then filtered and washed several times with hot distilled water until pH 7. Finally, the sample was dried in an oven for 12 h at 100 °C and calcined at 450 °C in air for 18 h to obtain the MgO-Al_2O_3 mixed oxide.

10 wt% Cu/MgO was prepared by an incipient wet impregnation method using the required quantity aqueous solution of Cu $(NO_3)_2 \cdot 3H_2O$ as a metal precursor. The resulting slurry was stirred well on a hot plate to remove the excess water and subsequently dried in an oven at 100 °C for 12 h. The solid residue was then crushed and calcined in air at 450 °C for 5 h and labeled 10CM. Similarly, 10 wt% Cu/Al_2O_3, 10 wt% Cu/MgO-Al_2O_3, and 10 wt% Cu/SiO_2 were prepared and assigned as 10CA, 10CMA, and 10CS, respectively.

2. Activity Studies

Coupling of the selective hydrogenation of NB to AN and the dehydrogenation of BDO to GBL involved using a fixed-bed down flow reactor (1 cm i.d, and 20 cm long) in the vapor phase under atmospheric pressure using various supported copper catalysts: 10CM, 10CA, 10CMA, and 10CS catalysts. Approximately 0.5 g of catalyst was used for all experiments and activated under flowing H_2 at 280 °C for 3 h at a flow rate of 60 ml min^{-1}. For the individual reactions, BDO or NB was fed at a flow rate of 1 ml h^{-1} under N_2 gas with a flow rate of 18 ml min^{-1}. In the NB to AN reaction, H_2 gas was used as a reducing gas with a H_2 and NB ratio of 3 : 1, respectively. For the coupling process, the NB to BDO ratio was maintained at 2 : 3 under N_2 flowing at 18 ml min^{-1}. The product mixture was collected from the outlet of the reactor in an ice-cold

Table 1. Physicochemical characterization of different supported copper catalysts

Catalysts	BET surface area ($m^2 g^{-1}$)	Cu content, XRF wt%	N_2O decomposition		d_{Cu} (nm) (XRD)	XPS Cu^0/Cu^{2+}	TPD of NH_3	
			Copper dispersion (%)	Copper particle size (nm)			Weak acid sites (100 to 200 °C) (μmol/g)	Medium acid sites (300 to 500 °C) (μmol/g)
10CM	25	9.87	10.1	44	53	1.50	-ND-	130
10CA	120	10.13	14.4	28	45	1.65	223	250
10CMA	60	9.92	12.3	36	40	1.25	-ND-	190
10CS	150	9.83	18.5	22	30	2.02	108	75

trap every hour. The samples were analyzed by gas chromatography (GC, Shimadzu-17A) equipped with an FID detector and ZB-wax capillary column (30 mL×0.5 mm I.D×1 μF. T). Before regular analysis, the products were identified by gas chromatography-mass spectrometry (GC-MS, Shimadzu-QP 5050) equipped with a DB-5 capillary column (30 mL×0.32 mm I.D×1 μF. T). The conversion of NB and BDO and the yield of AN and BDO were calculated using the following equations.

$$\text{Conversion (\%)} = (\text{Nitrobenzene or BDO intial weight} - \text{Nitrobenzene or BDO final weight}) / \text{Nitrobenzene or BDO intial weight} \times 100$$

$$\text{Yield (\%)} = \frac{\text{Conversion} \times \text{Selectivity}}{100}$$

RESULTS AND DISCUSSION

1. Catalyst Characterization

Table 1 lists the BET surface area and copper particle size for all catalysts. The surface areas of MgO, γ-Al_2O_3, MgO-Al_2O_3, and SiO_2 were 42, 180, 80, and 380 $m^2 g^{-1}$, respectively; the surface areas of the catalysts were lower than that of the corresponding bare supports. Among the catalysts, 10CM had the lowest surface area, i.e., 25 $m^2 g^{-1}$, whereas 10CS was 150 $m^2 g^{-1}$. The decrease in surface area of the catalysts compared to the supports was attributed mainly to the pore blockage of the support by the copper oxide particles [23].

The Cu content measured by XRF spectroscopy was maintained at 10 wt%. The dispersion of copper measured using the dissociative N_2O pulse method was in the range between 10.1 to 18.5% from 10CM to 10CS. The high dispersion of copper apparently leads to a decrease in particle size. Hence, among the catalysts, the smallest copper particles (ca. 22 nm) were observed over silica-supported copper catalyst. These results were collaborated by XRD (X-ray line broadening method), which showed a similar trend in the particle size. On the other hand, the particle sizes of copper measured by N_2O decomposition on the reduced catalyst were slightly different from those determined by XRD in an open atmosphere [23].

Fig. 1 shows the crystalline phases in the fresh and reduced catalysts determined by XRD. The crystallinity (D) of copper particle is calculated using Debye-Scherrer equation. $D = \frac{K\lambda}{\beta \cos\theta}$, where D=mean crystallite diameter, K=Scherrer's constant, λ=X-ray wave length (1.5418 Å for Cu Kα radiation), β=full width at half maximum and θ=diffraction angle. The XRD peaks at 35.5, 38.7, and 48.5° 2θ indicate crystallite CuO in the fresh catalysts (JCPDS file no. 48-1548), whereas the peaks at 43.29, 50.5, and 74.5° 2θ were assigned to metallic copper in the reduced catalysts (JCPDS file no. 03-1005). The remaining major XRD peaks of each catalyst corresponded to their supports. MgO (43.6, 62.2, 74.5, and 78.5° 2θ) has high crystallinity (JCPDS file no. 04-829) and SiO_2 (24° 2θ)

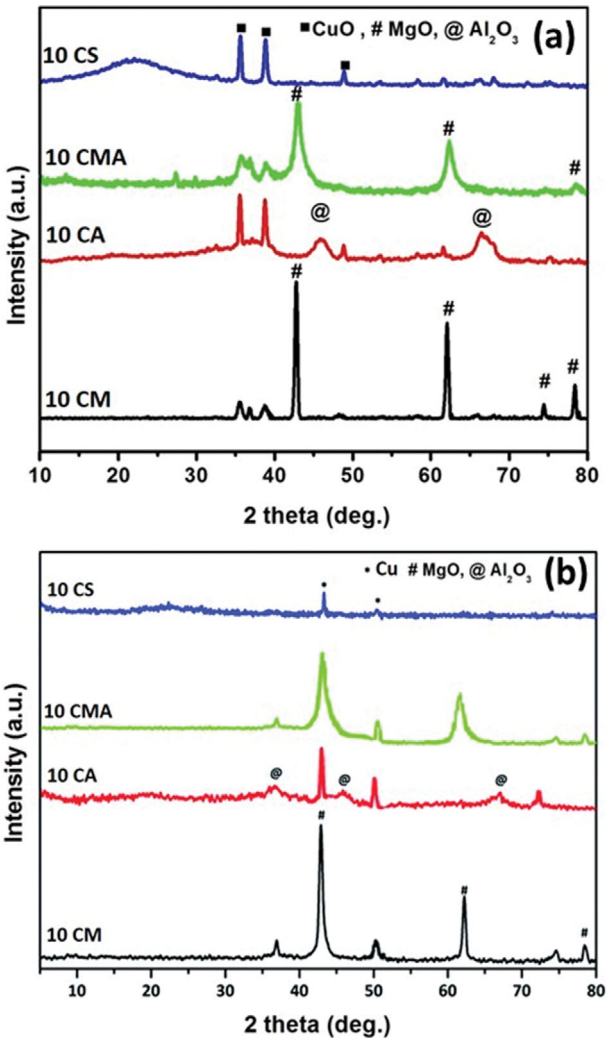

Fig. 1. XRD patterns of calcined (a) and reduced (b) of various supported copper catalysts.

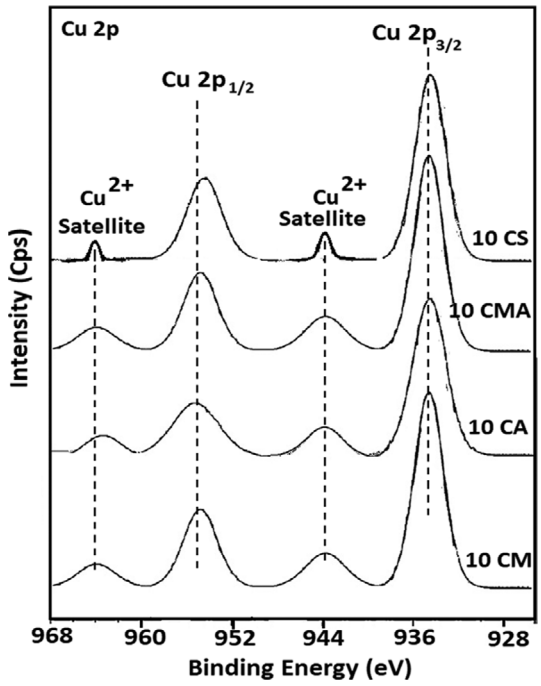

Fig. 2. XPS of Cu 2p patterns of various supported copper catalyst.

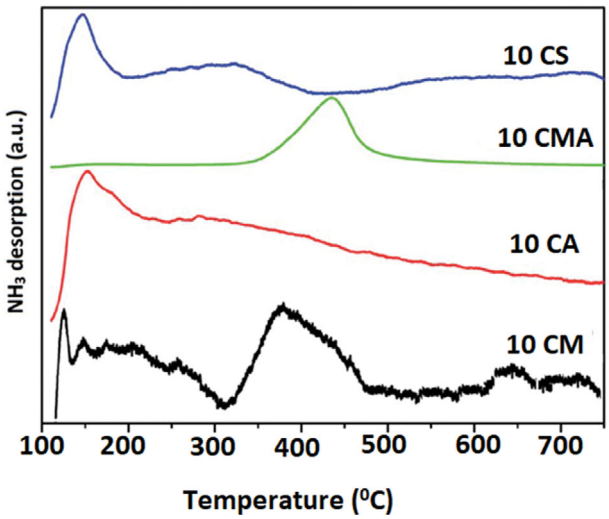

Fig. 3. NH_3 TPD patterns of various supported copper catalyst.

has very poor crystallinity, due mainly to its amorphous nature. The 10CMA catalyst showed mainly MgO XRD peaks, whereas alumina showed few peaks, indicating an amorphous form in the presence of MgO.

Fig. 2 presents the XPS spectra of supported Cu catalysts. The Cu 2p spectra showed two peaks associated with the Cu $2p_{3/2}$ (930-935 eV) and Cu $2p_{1/2}$ (952-958 eV). The binding energy (BE) of Cu $2p_{3/2}$ appeared at 933.671, 933.46, 933.59, and 932.87 eV for 10CM, 10CA, 10CMA, and 10CS, respectively. The binding energy at 944 eV corresponds to the satellite peak of Cu $2p_{3/2}$, which was assigned to Cu^{2+}. The satellite peaks were formed by ligand to metal 3d charge transfer, which is characteristic of Cu^{2+} compounds and is not observed in Cu^{+} [16]. The interaction of the metal and support and the metal particle size can affect the electronic character of the metal phase with the associated shifts in BE [16]. Table 1 lists the Cu^0/Cu^{2+} ratio calculated from XPS. The results showed that a larger amount of Cu^{2+} species was available on 10CM, whereas a smaller amount of Cu^{2+} species was observed on 10CS. Interestingly, the ratio was higher in 10CMA than 10CM but lower than 10CA, indicating that MgO does not stabilize the copper metal in 10CMA.

Fig. 3 shows the NH_3 TPD patterns for all supported copper catalysts. From the TPD profiles, the acid sites were identified as weak

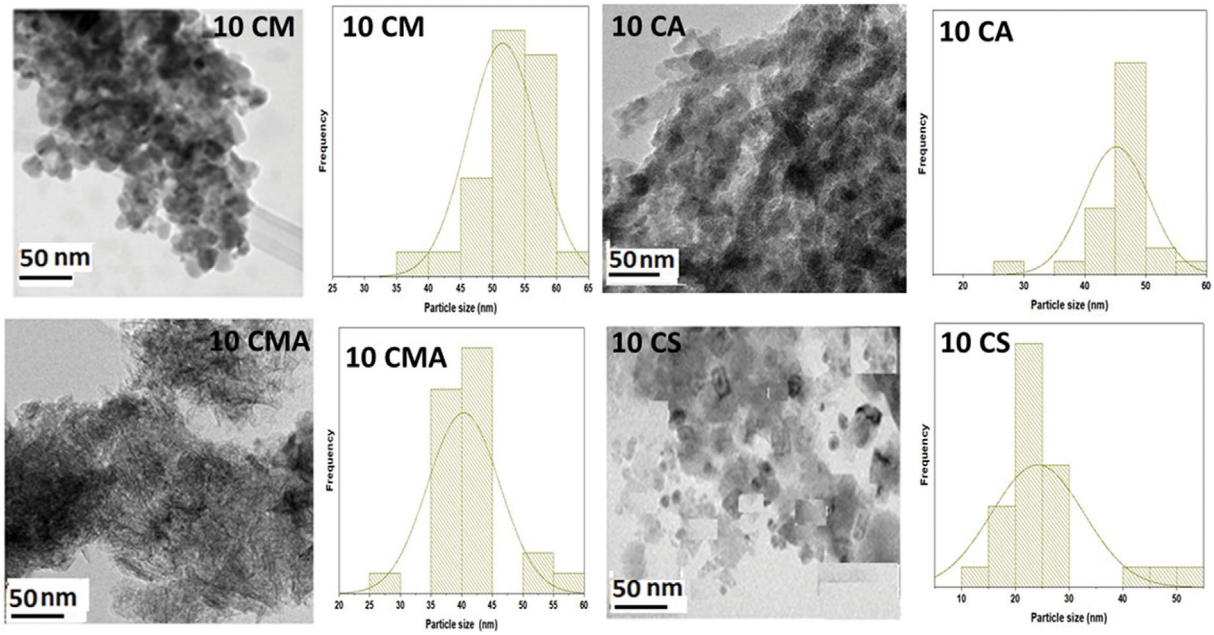

Fig. 4. TEM analysis and particle size distribution of various supported copper catalysts.

and medium acid sites based on NH_3 desorption. NH_3 desorption occurring from 100 to 200 °C was attributed to weak acid sites, whereas the desorption of NH_3 was observed from 300 to 500 °C, corresponding to the medium acid sites. MgO is a base support, so there are almost no weak acid sites and very few medium acidic sites (ca., 130 μmol/g). In particular, 10CA contained a high number of acidic sites (250 μmol/g) because of the acid nature of the support. Interestingly, 10CMA catalyst did not contain weak acid sites, but 190 μmol/g of medium acid sites were observed. A larger number of weak acid sites were observed for the 10CS catalysts, indicating the weak acidic nature of SiO_2.

Fig. 4 displays the TEM analysis of various supported copper catalysts. From the results, copper particles are uniformly distributed on supports. The 10CM catalyst presents cubic shape particles in the range of 35 to 65 nm and avg. particle size is 55 nm. In the case of 10CA, the particles seem to be cylindrical with a particle size of 45 nm. MgO-Al_2O_3 mixed oxide catalyst has needle-type particles and the average particle is 38 nm. Finally, copper particles are clearly seen in 10CS catalysts, and this indicates the weak interaction of SiO_2 and copper compared to other supported copper catalyst with the avg. 20 nm particle size of copper. Hence, the activity of the catalysts is also associated with the particle size of copper. The particle size of copper calculated from TEM analysis and XRD using Debye-Scherrer equation follows similar trend, supporting the agreement of both techniques.

2. Activity Studies

As shown in Scheme 1 (Eq. (1)), the BDO to GBL reaction was carried out under flowing N_2 (18 ml min^{-1}) over 10CM, 10CA, 10CMA, and 10CS at 250 °C. Fig. 5 shows the conversion and selectivity results. The catalysts used for the BDO transformation had different catalytic activity regardless of the active metal. BDO was converted to GBL and tetrahydrofuran (THF) products. The conversion of BDO to GBL occurred mainly only over 10CM and 10CS. In the case of 10CMA and 10CA, the BDO transformation proceeded by two pathways. THF formed via the dehydration of BDO as a major product over 10CA, whereas 10CMA produced

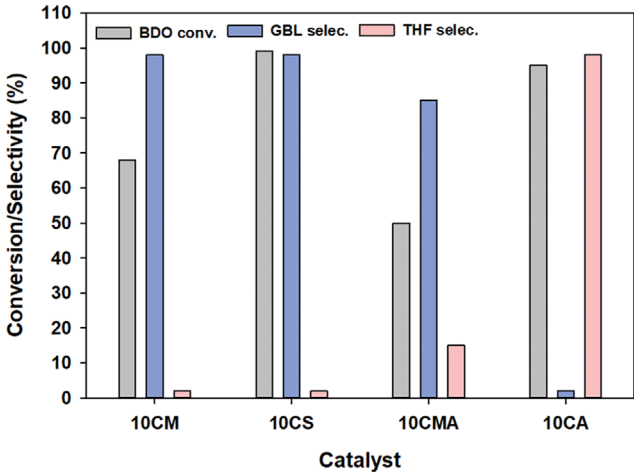

Fig. 5. BDO transformation over supported copper catalysts at 250 °C. Reaction conditions: catalyst weight=0.5 g, flow rate of BDO=1 ml h^{-1} and N_2=18 ml min^{-1}.

85% GBL and 15% THF. This shows that the formation of GBL and THF from BDO is associated with the total acidic sites of the catalyst. The order of acidity was as follows: 10CM<10CS<10CMA< 10CA. On the other hand, 10CS exhibited superior activity with 95% conversion of BDO and 98% selectivity of GBL.

Scheme 1 (Eq. (2)) represents the hydrogenation of NB over different supported copper catalysts (10CMI, 10CA, 10CMA, and 10CS) in flowing H_2 (18 ml min^{-1}) under atmospheric pressure at 250 °C; results are in Fig. 6. As shown, AN was the major product from the hydrogenation of NB over all catalysts. The NB to AN conversion rate was as follows: 10CS>10CM>10CA>10CMA. The selectivity of AN was not affected by the support, showing that both the acid and base supports are more favorable for AN formation [3-6]. The conversion of NB depends on the nature of the support because moderate acid sites are more favorable. The SiO_2-supported catalyst performance was high because of the larger num-

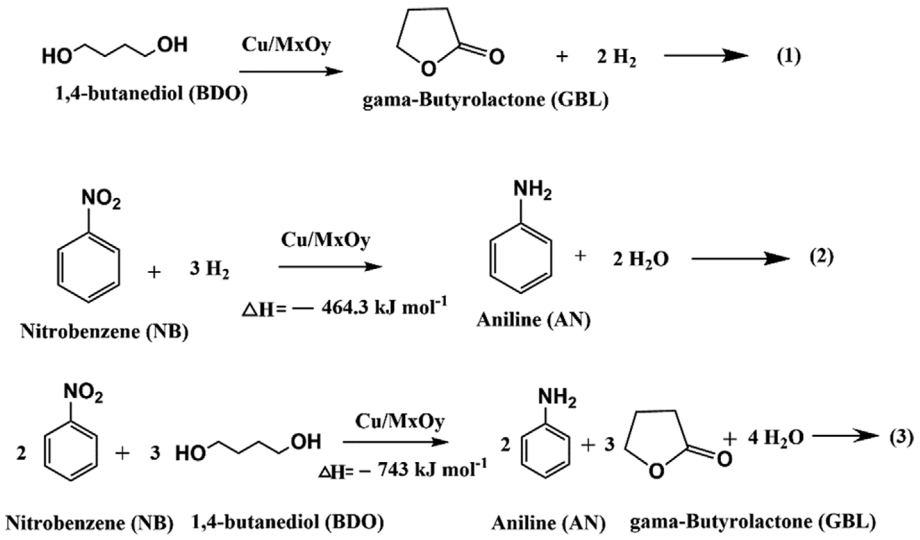

Scheme 1. Coupling of BDO dehydrogenation and NB hydrogenation over the supported copper catalysts.

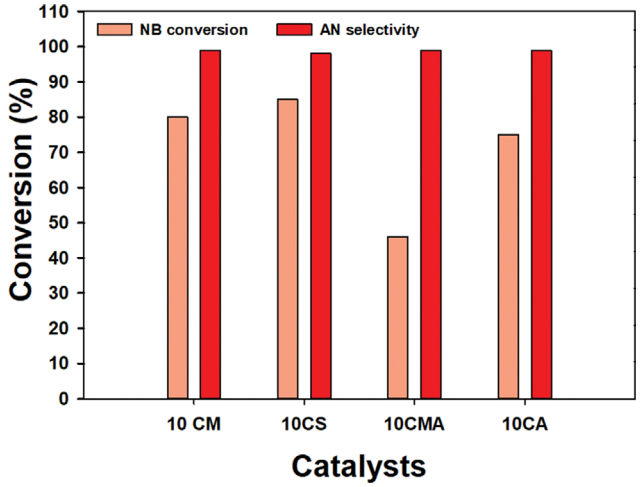

Fig. 6. NB hydrogenation over supported copper catalysts at 250 °C. Reaction conditions: catalyst weight=0.5 g, flow rate of NB= 1 ml h^{-1} and H_2=18 ml min^{-1}.

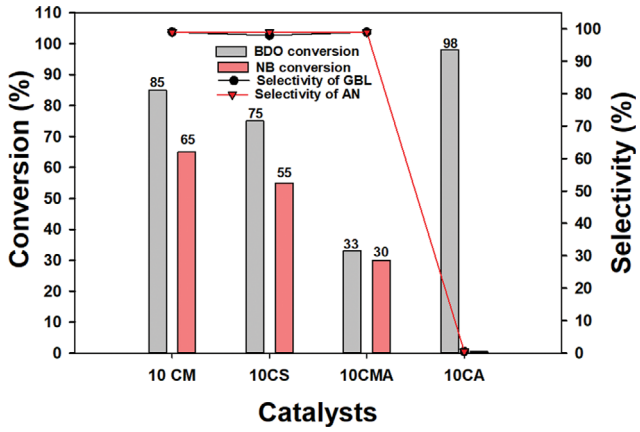

Fig. 7. Simultaneous BDO dehydrogenation and NB hydrogenation over supported copper catalysts at 250 °C. Reaction conditions: 0.5 g catalyst (red. H_2), NB and BDO (2 : 3) mixture=1 ml h^{-1} and N_2=18 ml min^{-1}.

ber of active sites, even though the acidity was low. According to Scheme 1 (Eq. (3)), coupling of the BDO dehydrogenation and NB hydrogenation (3 : 2 mole ratios) reactions was carried out under flowing N_2 (18 ml min^{-1}) in a fixed bed reactor over the supported copper catalysts at 250 °C.

Fig. 7 shows coupling reaction results at 250 °C over all four copper based catalysts. The coupling of BDO dehydrogenation and NB hydrogenation produced AN and GBL selectively. The activity result over 10CM catalyst showed 85% and 65% conversion of BDO and NB, respectively. Approximately 75% BDO and 55% NB conversions were observed with the 10CS catalyst. In contrast, the performance of 10CMA was poor because of larger copper particles, as observed from N_2O decomposition. In the case of 10CA, BDO transformed to THF because of its high acidic nature. Hence, no hydrogen production was observed from this reaction. Consequently, NB does not transform to AN under these conditions. The conversion of NB was >5% when the NB hydrogenation reaction was conducted with a stoichiometric amount of hydrogen. On the other hand, NB conversion increased from 5% to 85% over the 10CM catalyst when coupled with BDO dehydrogenation because of the basicity of the support. Among all supported copper catalysts, the 10CM catalyst showed more selectivity towards AN because MgO has high adsorption ability of hydrogen [7]. The coupling activity order for the different supported copper catalysts was 10CM>10CS>10CMA>10CA.

The superior performance of 10CM in coupling process is mainly attributed to the copper particle size (*ca.* 55 nm), which is higher than the other catalysts. In addition, MgO support showed only moderate acidic sites (130 μmol/g), suggesting that high basic sites are involved in hydrogen production and hydrogenation reaction. It was proposed that MgO alone can produce hydrogen from dehydrogenation of alcohols, while ethanol dehydration is a major reaction for Al_2O_3 [24]. Further, it was proposed that ion disorder generated at the grain boundaries of MgO could stabilize the hydrogen entities formed on catalyst surface, facilitating the formation of further higher alcohols [25]. Moreover, MgO is unique metal oxide that can dissociate hydrogen into H^+ and H^-, called as frustrated Lewis pair, and was found in MgO supported Ru catalyst [7]. Kim et al. [7] also described H_2 adsorption in two different ways, such as homolytic adsorption on metallic site and heterolytic adsorption on the surface of oxygen of MgO and Ru that is intimately contacted with MgO; as a result of that, low temperature hydrogenation occurred. In the present study, the Cu on MgO behavior was similar on hydrogen transfer reaction and well supported the higher performance of 10CM catalyst on hydrogenation of NB and dehydrogenation of BDO than other catalysts. XPS analysis of copper revealed that high BE of copper indicated strong interactions with MgO over Al_2O_3, MgO-Al_2O_3 and SiO_2 whose binding energies are lower, and further indicating that interactions between copper and support are weak. XPS analysis of 10CS has only one BE at 932.7 eV, further confirming there is no other chemical species of Cu phyllosilicates [26] with high Cu^0/Cu^{+2} of 2.02, indicating more surface copper active sites. But TPD of NH_3 showed high weak acidic sites than moderate sites. This could be the reason for less activity of 10CS and weak hydrogen adsorption capacity than 10CM. In the case of 10CA, copper particles size 45 nm with high amount of acid sites favoring dehydration of BDO to THF, indicating no hydrogen in the system for further hydrogenation of NB. Finally, for 10CMA which is a combination of MgO and Al_2O_3, the catalytic performance in coupling process is higher than individual 10CA but lower than 10CM, implying these mixture oxides did not enhance the activity.

CONCLUSIONS

The coupling reaction between BDO dehydrogenation and NB hydrogenation over different supported copper catalysts showed that the 10CM catalyst exhibits superior activity followed by 10CS and 10CMA. Furthermore, the individual BDO dehydrogenation to GBL conducted over 10CS was best compared to the other catalysts. In contrast, the high acidic nature of 10CA only produced THF both in a single and coupled reaction, suggesting that it is unsuitable for the present coupling process. Consequently, the cat-

alytic performance of various catalysts is dependent on the nature of the support (surface area, acidic and basic character) as well as the number of active surface copper atoms and the particle size of copper. In summary, this coupling protocol will have an immense impact on the commercial-scale production of fine chemicals.

ACKNOWLEDGEMENTS

Authors thank the Council of Scientific and Industrial Research-University of Grant Commission, New Delhi, India for granting the fellowship. This research was also supported by the National Research Foundation of Korea (NRF-2020R1I1A1A01073111).

SUPPORTING INFORMATION

Additional information as noted in the text. This information is available via the Internet at http://www.springer.com/chemistry/journal/11814.

REFERENCES

1. H. P. R. Kannapu, C. A. Mullen, Y. Elkasabi and A. A. Boateng, *Fuel Process. Technol.*, **137**, 220 (2015).
2. F. Zhao, Y. Ikushima and M. Arai, *J. Catal.*, **224**, 479 (2004).
3. C. S. Couto, L. M. Madeira, C. P. Nunes and P. Araujo, *Chem. Eng. Technol.*, **38**(9), 1625 (2015).
4. J. Wang, Z. Yuan, R. Nie, Z. Hou and X. Zheng, *Ind. Eng. Chem. Res.*, **49**, 4664 (2010).
5. X. Sun, O.-S. Alma I, O. Dmitrii, J. V. R Maria, K. Freek and G. Jorge, *J. Catal.*, **357**, 20 (2018).
6. H. P. R. Kannapu, R. Rahul, S. S. V. Reddy, D. R. Burri and K. S. Rama Rao, *Catal Commun.*, **10**, 879 (2009).
7. T. W. Kim, M. Kim, S. K. Kim, Y. N. Choi, M. Jung, H. Oh and Y.-W. Suh, *Appl. Catal. B: Environ.*, **286**, 119889 (2021).
8. D. W. Hwang, P. Kashinathan, J. M. Lee, J. H. Lee, U. Lee, J.-S. Hwang, Y. K. Hwanga and J.-S. Chang, *Green Chem.*, **13**, 1672 (2011).
9. K. H. P. Reddy, Y.-W. Suh, A. Narani, D. R. Burri and K. S. R. Rao, *Catal. Lett.*, **147**, 90 (2017).
10. U. G. Hong, H. W. Park, J. Lee, S. Hwang and I. K. Song, *J. Ind. Eng. Chem.*, **18**, 462 (2012).
11. H. Jeong, T. H. Kim, K. I. Kim and S. H. Cho, *Fuel Process Technol.*, **87**, 497 (2006).
12. G. Dezhi, F. Yonghai, Y. Hengbo, W. Aili and J. Tingshun, *Chem. Eng. J.*, **233**, 349 (2013).
13. A. Kuksal, E. Klemm and G. Emig, *Stud. Surf. Sci. Catal.*, **130**, 2111 (2000).
14. S. Satoshi, I. Jun and Y. Yasuhiro, *Appl. Catal. A: Gen.*, **453**, 213 (2013).
15. M. Li, Y. Hao, C.-L. Fernando, H. H. P. Yiu and A. K. Mark, *Top Catal.*, **58**, 149 (2015).
16. Z. Jian, S. Kai, A. Zhe, Z. Yanru, S. Xin, S. Hongyan, X. Xu and H. Jing, *Ind. Eng. Chem. Res.*, **59**, 3342 (2020).
17. M. A. Aramendia, V. Borau, C. Jimenez, J. M. Marinas, A. Porras and F. J. Urbano, *J. Catal.*, **161**, 829 (1996).
18. H. Ren, C.-H. Xu, H.-Y. Zhao, Y.-X. Wang, J. Liu and J.-Y. Liu, *J. Ind. Eng. Chem.*, **28**, 261 (2015).
19. B. S. Coluccia, F. Boccuzzi, G. Ghiotti and C. Morterr. *J. Chem. Soc., Faraday Trans.*, **I**, **78**, 2111 (1982).
20. G. Wu, J. Zhang, Y. Wu, Q. Li, K. Chou and X. Bao, *J. Alloys Compd.*, **480**, 788 (2009).
21. V. Mohan, C. V. Pramod, M. Suresh, K. Hari Prasad Reddy, B. David Raju and K. S. Rama Rao, *Catal. Commun.*, **18**, 89 (2012).
22. G. Lee, J. Y. Kang, N. Yan, Y.-W. Suh and J. C. Jung, *J. Mol. Catal. A: Chem.*, **423**, 347 (2016).
23. H. P. R. Kannapu, N. C. K. Prasad, K. S. R. Rao, V. N. Kalevaru, A. Martin and D. R. Burri, *Catal. Sci. Technol.*, **6**, 5494 (2016).
24. N. Takezawa, C. Hanamaki and H. Kobayashi, *J. Catal.*, **38**, 101 (1975).
25. E. Hemo, R. Virduk, M. V. Landau and M. Herskowitz, *Chem. Eng. Trans.*, **21**, 1243 (2010).
26. H. Li, L. Ban, Z. Wang, P. Meng, Y. Zhang, R. Wu and Y. Zhao, *Nanomaterials*, **9**, 842 (2019).